Article

Embedding Fragment ab Initio Model Potentials in CASSCF/CASPT2 Calculations of Doped Solids: Implementation and Applications

Ben Swerts, Liviu F. Chibotaru, Roland Lindh, Luis Seijo, Zoila Barandiaran, Sergiu Clima, Kristin Pierloot, and Marc F. A. Hendrickx

J. Chem. Theory Comput., **2008**, 4 (4), 586-594 • DOI: 10.1021/ct7003148 • Publication Date (Web): 05 March 2008

JCTC Journal of Chemical Theory and Computation

Embedding Fragment ab Initio Model Potentials in CASSCF/CASPT2 Calculations of Doped Solids: Implementation and Applications

Ben Swerts,[†] Liviu F. Chibotaru,*[,†] Roland Lindh,[‡] Luis Seijo,[§] Zoila Barandiaran,[§] Sergiu Clima,[†] Kristin Pierloot,[†] and Marc F. A. Hendrickx[†]

Division of Quantum and Physical Chemistry, Katholieke Universiteit Leuven, Celestijnenlaan 200F, B-3001 Heverlee, Belgium, Department of Theoretical Chemistry, Chemical Center, Lund University, P.O. Box 124, 221 00 Lund, Sweden, and Departamento de Química, C-14, and Instituto Universitario de Ciencia de Materiales Nicolás Cabrera, Universidad Autónoma de Madrid, 28049 Madrid, Spain

Received November 17, 2007

Abstract: In this article, we present a fragment model potential approach for the description of the crystalline environment as an extension of the use of embedding ab initio model potentials (AIMPs). The biggest limitation of the embedding AIMP method is the spherical nature of its model potentials. This poses problems as soon as the method is applied to crystals containing strongly covalently bonded structures with highly nonspherical electron densities. The newly proposed method addresses this problem by keeping the full electron density as its model potential, thus allowing one to group sets of covalently bonded atoms into fragments. The implementation in the MOLCAS 7.0 quantum chemistry package of the new method, which we call the embedding fragment ab inito model potential method (embedding FAIMP), is reported here, together with results of CASSCF/CASPT2 calculations. The developed methodology is applied for two test problems: (i) the investigation of the lowest ligand field states $^2A_1$ and $^2B_1$ of the Cr(V) defect in the YVO_4 crystal and (ii) the investigation of the lowest ligand field and ligand–metal charge transfer (LMCT) states at the Mn(II) substitutional impurity doped into $CaCO_3$. Comparison with similar calculations involving AIMPs for all environmental atoms, including those from covalently bounded units, shows that the FAIMP treatment of the YVO_4 units surrounding the CrO_4^{3-} cluster increases the excitation energy $^2B_1 \rightarrow {}^2A_1$ by ca. 1000 cm^{-1} at the CASSCF level of calculation. In the case of the $Mn(CO_3)_6^{10-}$ cluster, the FAIMP treatment of the CO_3^{2-} units of the environment give smaller corrections, of ca. 100 cm^{-1}, for the ligand-field excitation energies, which is explained by the larger ligands of this cluster. However, the correction for the energy of the lowest LMCT transition is found to be ca. 600 cm^{-1} for the CASSCF and ca. 1300 cm^{-1} for the CASPT2 calculation.

I. Introduction

When using the molecular orbital (MO) approach for the description of local properties of crystals, one has to take special care because of their periodic nature. The MO method of choice is normally applied to a representative part of the structure, usually a part of the unit cell, but the effects of the infinite environment cannot be ignored. All proposed solutions are based on the principles of localization and the separability of a many-electron system into subsystems. One of the simplest solutions was pioneered by Sugano and Shulman.[1] They surrounded the structure with point charges to reproduce the electrostatic potential. In the field of organic

* Corresponding author phone: +32-16-327424; fax: +32-16-327992; e-mail: Liviu.Chibotaru@chem.kuleuven.be.

[†] Katholieke Universiteit Leuven.

[‡] Lund University.

[§] Universidad Autónoma de Madrid.

10.1021/ct7003148 CCC: $40.75
Published on Web 03/05/2008

crystal research, this principle was extended to the super molecule[2] (SM) and quantum mechanics/molecular mechanics (QM/MM)-based[3] models, which are of value in geometrical analysis. For the study of inorganic crystals, however, accurate SM-based models quickly become computationally too expensive because they include the nearest neighbors into the wave function. Crystals containing metals need to be described using larger basis sets and more accurate multiconfigurational expansions of the wave function. It is also beneficial to be able to limit any electron correlation treatment to the central part of the system.[4]

The embedding ab initio model potential (AIMP) method,[5] which proved to be successful in many applications,[6] addresses this by replacing the nearest neighbors by a set of frozen electron densities. These densities are represented by spherical model potentials centered on the atomic positions. Herein lies its major limitation: the environment cannot always easily be divided into spherical ions. When strongly covalently bonded structures are present, the resulting electron density is anisotropic and not accurately representable either by a set of spherical densities or a single large spherical density. A natural following step would be the generalization of the embedding AIMP method to covalently bounded groups of atoms (which we call fragments).

The fragment approach has a long history in quantum chemistry, and many versions of this approach have been proposed in the past. For instance, in the integrated ab initio plus molecular mechanics geometry optimization (IMMOM) method,[7] the chemical groups linked to the active site through a single bond are replaced by the hydrogen atom, while nonbonded interactions of the active site with other atoms in the molecule are described by the MM force field. More rigorous approaches are based on the theory of separability of many-electron systems consisting of weakly interacting parts[8,9] for which effective group potentials (EGPs) can be rigorously introduced. Thus, Katsuki[10] and Mejias Romero and Sanz[11] have developed EGPs for chemical groups linked to the active site by intermolecular interactions, without taking into account charge transfer effects. These effects are incorporated in the effective fragment potential (EFP) approach, which includes a small basis set on the fragment, simulating the covalent interactions of some fragment electrons with the active site, while the interactions with other electrons of the fragment are described by a model potential. Ohta et al.[12] have proposed an EFP for the NH_3 groups which included only the lone pair orbital of the nitrogen in the basis set. von Arnim and Peyerimhoff[13,14] have developed an EFP version for small chemical groups where the short-range part of the potential is stored in an intermediate atomic orbital basis set and the long-range part of the potential is simulated by multipole expansions. Another version of this approach, proposed by Colle et al.,[15,16] uses the nonlocal representation for the short-range part of the fragment potential, including the short-range part of the Coulomb interaction, expressed via molecular orbitals of the fragment. An alternative approach is the EGP method introduced by Durand and Malrieu,[17] which is a shape-consistent potential aimed at the reproduction of the active valence orbitals of the fragment, rather than its entire effect on the active site, as was the goal of the EFP. The EGP method was developed by the Toulouse group[18] and proved to be often a reliable tool of fragment calculations of the molecules.[19]

In this article, we propose the embedding fragment ab inito model potential (embedding FAIMP) method, which is basically an extension of the conventional embedding AIMP over polyatomic groups. It uses exact potentials in the sense that a multiatom fragment can be treated as a single entity and is represented by its full electron density. When used with single atom fragments, the method is functionally identical to the embedding AIMP method. The details of the method are presented in the next section, and the details of its implementation into the MOLCAS-7.0 quantum chemistry software are given in section III. Then, in section IV, we apply this method for two substitutional impurity problems.

II. Method Description

The FAIMP method assumes some of the approximations of the AIMP method and improves other ones. In particular, FAIMP assumes the frozen environment approach (typical of embedding techniques), which makes it applicable only to the calculation of local properties, namely, those which depend strongly on the local geometry and electronic structure of a reference cluster and depend only secondarily on the electronic structure of the environment. The frozen environment approach is a basic assumption in the AIMP embedded cluster method, and although improvements including lattice relaxation and polarization have been explored,[6] it has been found that it is very accurate when applied to very ionic hosts where monatomic ions are easily distinguished. It is reasonable to expect that the frozen environment approach should equally apply to more complex hosts where ionic interactions also occur among fragments (which can be monatomic but also polyatomic ions), whereas covalent interactions may occur within the polyatomic fragments. In these cases, the existing covalent interactions within the polyatomic fragments should be adequately treated at the stage of generating the effective embedding potential, so that the effective potential corresponds to the electronic structure of a polyatomic density instead of corresponding to a set of monatomic electronic densities (examples of hosts of this type are YVO_4 and $CaCO_3$, treated in section IV). Otherwise, the interactions between the reference cluster and the external fragments are subject to the same approximations and, presumably, to the same accuracy, as in previous applications of the AIMP embedded cluster method. Consistently, the frozen fragment electronic structure would generate polyatomic Coulomb, exchange, and projection operators which can either be calculated explicitly, this being the alternative in the present implementation, or be subject to further approximation along the usual AIMP recipes for representing local and nonlocal operators, this being the target of future implementations. This latter step should result in significant savings in the evaluation of the FAIMP one-electron integrals in the cluster basis set.

II.1. The Energy Expression. For the derivation of the embedding FAIMP Hamiltonian, we consider a central cluster surrounded by a frozen environment consisting of

multiatom fragments. The many-electron nonrelativistic Hamiltonian of this system with $N_{clus} + N_{env}$ electrons reads

$$H_{tot} = \sum_{i}^{N_{clus}+N_{env}} \left\{ -\frac{1}{2}\nabla_i^2 - \sum_K \frac{Z_K}{|r_i - R_K|} \right\} + \sum_{i>j}^{N_{clus}+N_{env}} \frac{1}{r_{ij}} + \sum_{K>L} \frac{Z_K Z_L}{|R_K - R_L|} \quad (1)$$

Within the theory of separability of many-electron systems (group-function theory),[8,9] the total wave function for the system is written as a generalized antisymmetric product of group wave functions. Each group wave function can be a single or multiconfigurational expansion with the added limitation that the number of electrons in each group is constant. This means any electron correlation or electron transfer between groups is ruled out. If the group wave functions fulfill the strong orthogonality condition,[20] the effective electronic Hamiltonian for a single group G can be written as

$$H_{eff}^G = H^G + \sum_i \sum_{L \notin G} \frac{Z_L}{|r_i - R_L|} + \sum_i \sum_{j \notin G} \frac{1}{r_{ij}} \quad (2)$$

It includes the interactions of the electrons of the group with the nuclei (core-attraction) and electrons (Coulomb repulsion and exchange) of all other groups. In practice, this equation cannot be used as-is, however, as its rigorous application would lead to variational collapse of the active electron orbitals onto the frozen orbital space of the fragments because the orthogonality conditions are not imposed. They can be applied following the procedure by Huzinaga and Cantu.[6,8]

As most solutions of the many-electron Hamiltonian are based on orbital expansions, we assume for simplicity that we are dealing with a closed-shell Hartree–Fock (HF) calculation. In this case, the orbitals are solutions of the following Fock equation:

$$F_{tot}|\varphi_i\rangle = \left\{ -\frac{1}{2}\nabla^2 - \sum_K \frac{Z_K}{|r - R_K|} + \sum_j (2J_j - K_j) \right\} |\varphi_i\rangle = \epsilon_i |\varphi_i\rangle \quad (3)$$

Now, when we split the system into cluster and environment electrons, subject the orbitals to the following orthogonality conditions:[6,8]

$$\langle \varphi_i^{env} | \varphi_j^{env} \rangle = \delta_{ij} \qquad \langle \varphi_i^{clus} | \varphi_j^{env} \rangle = 0 \qquad \langle \varphi_i^{clus} | \varphi_j^{clus} \rangle = \delta_{ij} \quad (4)$$

and minimize the total energy under the variational restriction that φ^{env} remain frozen, we obtain

$$\left\{ F^{tot} - \left[\sum_{env} |\varphi^{env}\rangle\langle\varphi^{env}| F^{tot} + F^{tot} \sum_{env} |\varphi^{env}\rangle\langle\varphi^{env}| \right] \right\} |\varphi^{clus}\rangle = \epsilon^{clus} |\varphi^{clus}\rangle \quad (5)$$

Then, if we choose the frozen environment orbitals to be eigenfunctions of F^{tot}, we obtain a Huzinaga−Cantu-like equation: [6,8]

$$\left\{ F^{tot} + \sum_{env} (-2\epsilon^{env}) |\varphi^{env}\rangle\langle\varphi^{env}| \right\} |\varphi^{clus}\rangle = \epsilon^{clus} |\varphi^{clus}\rangle \quad (6)$$

Combining this with group-function theory, we obtain the following Hamiltonian for the central cluster:

$$H_{eff}^{clus} = H^{clus} + \sum_i^{N_{clus}} \sum_{L \in env} \frac{Z_L}{|r_i - R_L|} + \sum_i^{N_{clus}} \sum_j^{N_{env}} \frac{1}{r_{ij}} + \sum_F^{N_{frag}} \sum_{o \in F}^{occ} (-2\epsilon_o) |\varphi_o^F\rangle\langle\varphi_o^F| \quad (7)$$

with $\varphi_0{}^F$ being an occupied orbital of fragment F and N_{frag} the number of fragments in the system.

The first two correction terms are trivial to implement, but the last term (the projection operator) needs to be rewritten in linear combination of atomic orbitals (LCAO) form, based on the expansion $\varphi_o^F = 2\sum_{\lambda \in F} c_{o\lambda} \lambda$ $\varphi_o = \sum_{\lambda \in F} c_{o\lambda} \lambda$ and the expression for the energy-weighted density matrix $W_{\lambda\sigma} = 2\sum_{o \in F}^{occ} \epsilon_o c_{o\lambda} c_{o\sigma}$:

$$\begin{aligned} H_{\mu\nu}^{proj} &= \sum_F \sum_{o \in F}^{occ} (-2\epsilon_o) \langle \mu | \varphi_o^F \rangle \langle \varphi_o^F | \nu \rangle \\ &= \sum_F \sum_{o \in F}^{occ} \sum_{\lambda\sigma \in F} (-2\epsilon_o) c_{o\lambda} c_{o\sigma} \langle \mu | \lambda \rangle \langle \sigma | \nu \rangle \\ &= -\sum_F \sum_{\lambda\sigma \in F} W_{\lambda\sigma}^F \langle \mu | \lambda \rangle \langle \sigma | \nu \rangle \end{aligned} \quad (8)$$

Noting that, in this and the following expressions, the indices μ and ν loop over the basis functions of the cluster and the indices λ and σ loop over the basis functions of the fragments F (which means both indices should always point to basis functions of the same fragment),[21] the complete electronic energy can be written in LCAO form:

$$E^{clus,eff} = E^{clus} + \sum_{\mu\nu} D_{\mu\nu} \left\{ \sum_{L \in env} \left\langle \mu \left| \frac{Z_L}{|r - R_L|} \right| \nu \right\rangle + \sum_{\lambda\sigma} D_{\lambda\sigma}^F (\mu\nu || \lambda\sigma) - \sum_{\lambda\sigma} W_{\lambda\sigma}^F \langle \mu | \lambda \rangle \langle \sigma | \nu \rangle \right\} \quad (9)$$

where the density matrices of the cluster and the fragments are defined as

$$D_{\mu\nu} = 2\sum_{o \in S}^{occ} c_{o\mu} c_{o\nu} \quad (10a)$$

and

$$D_{\lambda\sigma}^F = 2\sum_{o \in F}^{occ} c_{o\lambda} c_{o\sigma} \quad (10b)$$

respectively. When expression 9 is applied to fragments consisting of single atoms, the resulting energies are comparable to those obtained using the electronic embedding AIMP Hamiltonian. The energy of the AIMP embedded cluster, however, also contains an effective nuclear repulsion term between the nuclei in the cluster and in the environment:

$$E_{nuc}^{AIMP} = \sum_{K \in clus} \sum_{L \in env} \frac{Z_K Z_L}{R_{KL}} \quad (11)$$

II.2. First Derivatives of the Energy. In order to determine the first derivative of the full FAIMP Hamiltonian,

one first has to determine all constant terms: the fragments' orbital energies and coefficients and the fragment atoms' Mulliken charges. This leads to the following expression for taking the derivative with respect to the positions of the atoms of the central cluster $\{R\}$:

$$\frac{\partial E^{\text{clus,eff}}}{\partial R} = \frac{\partial E^{\text{clus}}}{\partial R} + \sum_{K\in\text{clus}}\sum_{L\in\text{env}} Z_K Z_L \frac{\partial R_{KL}^{-1}}{\partial R} + \sum_{\mu\nu} D_{\mu\nu}\left\{\sum_{K\in\text{env}} \frac{\partial}{\partial R}\left\langle\mu\left|\frac{Z_K}{|r-R_K|}\right|\nu\right\rangle + \sum_{\lambda\sigma} D^F_{\lambda\sigma}\frac{\partial}{\partial R}(\mu\nu\|\lambda\sigma) - \sum_{\lambda\sigma} W^F_{\lambda\sigma}\frac{\partial}{\partial R}\langle\mu|\lambda\rangle\langle\sigma|\nu\rangle\right\}\left[+\sum_{\mu\nu}\frac{\partial D_{\mu\nu}}{\partial R}\left\{\sum_{L\in\text{env}}\left\langle\mu\left|\frac{Z_L}{|r-R_L|}\right|\nu\right\rangle + \sum_{\lambda\sigma} D^F_{\lambda\sigma}(\mu\nu\|\lambda\sigma) - \sum_{\lambda\sigma} W^F_{\lambda\sigma}\langle\mu|\lambda\rangle\langle\sigma|\nu\rangle\right\}\right] \quad (12)$$

The last set of terms contains the derivative of the cluster's density matrix. Because the fragment orbitals are also eigenfunctions of F^{clus} (see eq 5), these terms should be added to similar terms occurring when determining the derivative of E^{clus} in the Hartree–Fock case.[23] This means they are also included in the term

$$-\sum_{\mu\nu} W_{\mu\nu}\frac{\partial S_{\mu\nu}}{\partial R} \quad (13)$$

already calculated in $\partial E^{\text{clus}}/\partial R$. This means that eq 12 is in principle only valid when the set of terms in square brackets is removed.

III. Implementation Details

The Hamiltonian of the considered system in the environment of fragments, represented by their full molecular density, can be expressed as follows:

$$H^{\text{FAIMP}}_{\mu\nu} = H_{\mu\nu} - \sum_E\left\langle\mu\left|\frac{Z_E}{|r-R_E|}\right|\nu\right\rangle + \sum_M\sum_{ab\in M} D^M_{ab}\left[(\mu\nu|ab) - \frac{1}{2}(\mu a|\nu b)\right] + \sum_M\sum_{A\in M}(-2\epsilon_A)\langle\mu|A\rangle\langle A|\nu\rangle$$

where $\mu\nu$ are the basis functions of the central cluster and ab are the basis functions on atoms E of each fragment M used to compute the fragment orbitals A and the density matrices $D_{ab}{}^M$. In the derivation of the energy expression, an all-electron description of the cluster is assumed. The energy expression is equally valid for usage with effective core potentials[6] if the core potential Hamiltonian is used instead of H^{clus}. The same argument can be used for the fragments. They can also be constructed using ECP-type basis sets. As in the regular case, only interaction integrals are calculated, so constant one-center contributions are omitted. Finally, the relativistic effects can be included in the same fashion as in the AIMP approach.[6]

The FAIMP energy and first derivatives are implemented in the MOLCAS 7.0 package.[24] After the geometry of the system is read, where the fragments are specified just as one center (which is normally taken to be an obvious location like the symmetry center or the center of mass), fragments

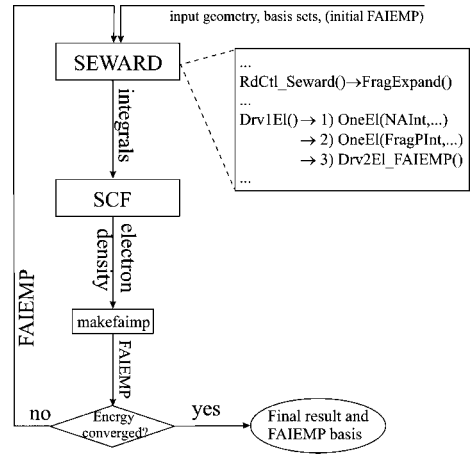

Figure 1. Flowchart of the FAIMP procedure implemented in the MOLCAS-7.0 package.

are expanded (new atoms created from the fragment's atoms) according to the specifications in the fragment density library, and all other data for the fragments are read. Several routines are modified/added to the SEWARD module from MOLCAS suite of programs to evaluate the fragment-related integrals (Figure 1), beside the regular integrals $H_{\mu\nu}$:

1.Nuclear attraction integrals between the cluster's electrons and the fragment nuclei of the expanded fragment atoms:

$$\sum_E \frac{Z_E}{r_\mu - R_E}$$

2.Projection integrals, which are assembled from energy-weighted density matrix $W_{\lambda\sigma}{}^M$ and the two overlap integrals $\langle\mu|\lambda\rangle$ and $\langle\sigma|\nu\rangle$ and contracted afterward. The results are added to the one electron Hamiltonian:

$$\begin{aligned} P^{\text{FAIMP}}_{\mu\nu} &= \sum_M\sum_{A\in M}(-2\epsilon_A)\langle\mu|A\rangle\langle A|\nu\rangle \\ &= \sum_M\sum_{A\in M}(-2\epsilon_A)\langle\mu|\sum_{\lambda\in M} c_{A\lambda}\lambda\rangle\langle\sum_{\lambda\in M} c_{A\lambda}\lambda|\nu\rangle \\ &= -\sum_M\sum_{\lambda\in M}\sum_{A\in M} 2\epsilon_A c_{A\lambda}c_{A\sigma}\langle\mu|\lambda\rangle\langle\sigma|\nu\rangle \\ &= -\sum_M\sum_{\lambda\sigma\in M} W^M_{\lambda\sigma}\langle\mu|\lambda\rangle\langle\sigma|\nu\rangle \end{aligned}$$

3.Two-electron interaction integrals. A relative efficiency is obtained with proper prescreening at this stage, by eliminating the intracluster and intra- and interfragment integrals and calculating only the cluster-fragment integrals. These are added locally to the one-electron Hamiltonian:

$$\sum_M\sum_{ab\in M} D^M_{ab}\left[(\mu\nu|ab) - \frac{1}{2}(\mu a|\nu b)\right]$$

With all one- and two-electron integrals computed, the SCF module computes a HF electronic density, from which a small utility (MAKEFAIMP) generates the fragment AIMP basis set. The resulting so-called FAIMP basis set can be included in the Fragment library, but it is not a regular basis

set. It consists of a standard name (X.FRAGMENT.author.0s.0s.0e-FAIMP-compoundName-etc), the name of the standard basis sets of the participating atoms, relative (to the positioning center that is specified in the input) coordinates of the fragment atoms, orbital energies and coefficients of the occupied fragment orbitals, and Mulliken charges on each atom of the fragment from the calculated SCF wave function. The fragment AIMP generated in this way for a particular crystalline environment can be used in other crystals as well, but when generated for the specific environment, it will give better results. It is, though, a good idea to use FAIMP from other crystals as a starting point for the considered environment. The possibility to perform geometry optimization is implemented in the ALASKA module, where the first derivatives are calculated in the way described above.

The fragment AIMP method was designed to be a generalization of the AIMP method,[5,6] and the same iterative procedure is used to obtain the fragments' orbital energies and coefficients so that (energy-weighted) density matrices are obtained that correspond to fragments in a perfect crystalline environment. The iterative procedure uses restricted Hartree–Fock calculations to obtain the basis sets. Methods incorporating electron correlation can be used too, though the equations are not formally valid for them and have not been tested. The starting point (when no FAIMPs are available to start with) is a single-point SCF calculation of each multiatom molecular fragment that can be considered as a single entity in the crystalline structure. The resulting total density of the fragment from the first single-point calculation is taken as the embedding fragment's basis set for the subsequent run. By alternating the different fragments on the position of a central cluster and employing densities from the previous steps as input for the embedding fragments, a new and improved electron density is generated. The central cluster is usually embedded in a few shells of FAIMP and eventually a few shells of point charges. The self-consistent iterative procedure continues until convergence (usually ~25–30 steps) and is implemented as a shell script, which can be concisely summarized as follows:

while [SCF Energy not converged]
do
for EachFragment *in* AllFragmentTypes
do
Molcas (SEWARD) compute integrals
Molcas (SCF) calculate SCF wavefunction
MAKEFAIMP generate FAIMP basis set out of the SCF wavefunction
done
done

The described implementation of the FAIMP method in the MOLCAS 7.0 package still lacks two essential features. First, it is not yet in the AIMP representation[6] but is still represented by a collection of bielectronic Coulomb and exchange integrals between cluster and fragment orbitals. In order to achieve the AIMP representation, the short-range Coulomb and exchange interaction should be represented via nonlocal operators, as it was proposed, for instance, for EFP by von Arnim and Peyerimhoff.[13,14] Second, the symmetry is not yet implemented for the FAIMP procedure.

The FAIMP is particularly suitable for ionic hosts formed by polyatomic ions or charged fragments, as commented upon above. Consequently, the fragment group functions are expected to be naturally localized within the fragment volume (the same is true for the reference cluster, as commented upon above). Thus, the basis set used to obtain the fragment molecular orbitals can be restricted to include only the bases of the atoms forming the fragment. This natural localization allows for the use of smaller fragment basis sets than the ones that would be presumably needed if standard Hartree–Fock calculations with (partly frozen) localized orbitals would be performed. The latter would be superior, however, in cases where the environment is not naturally localized, as it has been demonstrated in the study of defects and chemisorption in metallic surfaces.[25]

IV. Illustrative Calculations

In order to assess the importance of the FAIMP approach for the treatment of the effects of covalently bonded groups on the electronic structure of transition metal clusters, we made test calculations for two substitutional impurity systems: (i) YVO_4:Cr^{5+} and (ii) $CaCO_3$:Mn^{2+}. In both of these cases, no geometry optimization has been done. The main goal of these calculations was the comparison of FAIMP and AIMP approaches.

IV.1. Cr(V) Impurity in YVO_4 Crystal. Cr(V)-doped yttrium vanadate (YVO_4) is a member of a class of compounds with a potential use as tunable solid-state lasers. In this system, chromium has a high oxidation state, which has only been found to be stable in a tetraoxo coordination. If the CrO_4^{3-} structure was in a pure tetrahedral environment, it would have an ^2E ground state and a $^2T_2$ excited state several thousand wavenumbers higher in energy. The YVO_4 crystal, however, exhibits a distortion with an elongation along the binary axis[26] (in contrast with a more common compression along this axis),[27] lifting the degeneracy of the ^2E state. For the case of CrO_4^{3-}, crystal field theory (CFT) predicts the $^2B_1$ state ($d_{x^2-y^2}$) to be the ground state. EPR[28] and optical absorption[29] experiments, however, predict an $^2A_1$ (d_{z^2}) ground state. This is surprising, even more so considering the fact that the splitting of the $^2T_2$ state does occur as predicted by CFT.[29]

A number of explanations for this phenomenon have been proposed. It was suggested that it is due to strong covalency in the Cr−O bonding[28] or strong interactions with Y^{3+} ions in the second coordination sphere of chromium as revealed by DFT calculations.[29] A recent study by Pascual et al.[30] used CASSCF calculations on the CrO_4^{3-} cluster in combination with the AIMP method for the description of the crystalline environment. Their findings are in agreement with experiments regarding structure and ordering of the states. They concluded that the ordering is 76% due to direct and indirect embedding effects and 24% due to strong covalency. In order to do this type of calculation, the VO_4^{3-} ions had to be modeled as V^{5+} and O^{2-} ions, imposing spherical electron densities. A FAIMP description of the crystal is more in line with the nature of the crystal, as the entire fragment can be described as a single entity.

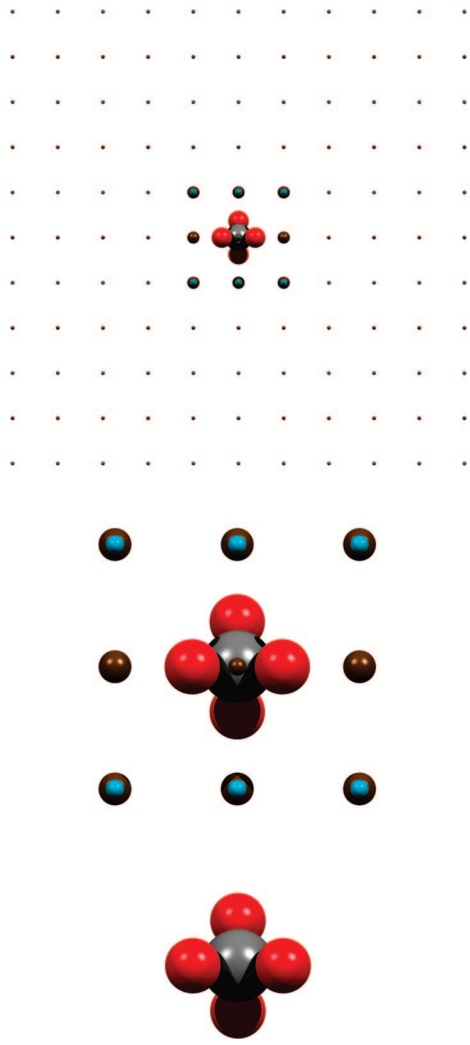

Figure 2. Schematic representation of the cluster CrO_4^{3-} (bottom) embedded into one layer of VO_4^{3-} FAIMP (small balls) and one layer of Y^{3+} AIMP (large balls) (middle) and eight layers of point charges (top). The view is along the 4-fold symmetry axis.

In the present study, the Cr(V) impurity in the YVO_4 crystal has been modeled by the CrO_4^{3-} central cluster surrounded by one layer of Y^{3+} and VO_4^{3-} fragments and eight layers of point charges in a $I4_1/amd$ crystalline structure reoriented to conform to a D_{2d} site symmetry (Figure 2). The geometry of the CrO_4^{3-} cluster was taken from ref 30 for the ground state $^2A_1$, where it was optimized in the embedded AIMP CASSCF calculation. The fragment densities were constructed and optimized for three entities: one for yttrium and two for two orientations of the vanadate ion, as the current MOLCAS implementation does not provide automatic rotation of fragments and their density matrices. The point charges have the values of the net charge of the fragments located at their fragment centers. The frontier charges were scaled according to Evjen's method[31] in order to attain a zero-charged environment.

For the description of the central CrO_4^{3-} cluster, two basis sets were used: The first was an ANO-RCC basis set,[32] contracted to [7s6p4d3f2g] for chromium and [4s3p2d1f] for oxygen and designated as "RCC" in the discussions. The second employed basis set, accompanying the core CG-AIMP by Barandiarán and Seijo,[33] was augmented with three f functions[34] and contracted as [4s4p5d1f] for chromium and [2s3p1d] for oxygen and referred to as "ECP". These are the same basis sets as used in a previous AIMP study by Pascual et al.,[30] thus allowing us to directly compare the present FAIMP results to these AIMP results. For the fragments, we constructed the FAIMP densities from three atomic basis sets, more specifically, an ANO-DK3 basis set[35] for all atoms (denoted as "DK3"), an ANO-RCC basis set, using a DZP contraction for all atoms (denoted as "RCC"), Cowan−Griffin relativistic core model potentials with a [3s3p4d] contraction of Barandiarán's AIMP[36] for yttrium, a [3s3p4d] contraction of Seijo's AIMP[37] for vanadium, and a [2s4p1d] contraction of Barandiarán's AIMP[33] for oxygen (denoted as "ECP"). The combinations of cluster basis and fragment basis sets will be denoted as RCC + DK3, RCC + RCC, and ECP + ECP. The FAIMP basis sets for the fragments were optimized to a convergence criterion of $\Delta E < 10^{-8}$ Hartree, which was achieved in 20–25 iterations, compared to an average of seven iterations for the atomic AIMP method.

The relative energies of the $^2A_1$ and $^2B_1$ states of the CrO_4^{3-} cluster were determined using the aforementioned combinations of basis sets using the CASSCF/CASPT2 method.[38–40] The active space consisted of the 3d orbitals of chromium and the 2p orbitals of the four oxygens for a total of 25 electrons in 17 active orbitals. The dynamical correlations were computed at the CASPT2 stage by correlating all but 1s of oxygen and 1s, 2s, and 2p electrons of Cr and V atoms. All ab initio calculations were performed with the MOLCAS 7.0 software.

The results for the first excitation energy are shown in Table 1. The calculated energies show a stronger dependence on the basis set in the case of a cluster embedded in the crystal than in the gas phase. This is especially the case for the CASPT2 calculations. The CASSCF excitation energy for the ECP + ECP basis can be compared directly with a similar AIMP calculation in ref 30, which gave a value of 1650 cm^{-1} for the direct $^2B_1 \rightarrow {}^2A_1$ gap. As we can see from Table 1, this result differs from the FAIMP calculation by ca. 1000 cm^{-1}. Although we cannot check the accuracy of these predictions by confronting them with experimental results, the obtained difference in the two approaches is large enough to justify the need for the FAIMP method in this case.

IV.2. Mn^{II} Impurity in Calcite. Divalent manganese in calcite is one of the most investigated substitutional impurities in molecular crystals. Calcite is the rhombohedral form of $CaCO_3$ and belongs to the space group D_{3d}^6.[41] There are two nonequivalent Ca(II) sites in the calcite corresponding to the alternation of the orientations of the CO_3^{2-} ions in the successive carbonate planes. The manganese(II) ions substituting the calcium(II) ions in calcite are octahedrally coordinated to six nearest-neighbor oxygen atoms of carbonate ions (Figure 3, bottom). Detailed structural investigations by X-ray standing waves and extended X-ray absorption fine structure (EXAFS) have shown[42] that the Mn−O distance is found to be the same as in the isostructural $MnCO_3$ (2.18 Å). Since this is shorter than the Ca−O distance in calcite

Table 1. Relative Energies (in cm^{-1}) of the Lowest $^2B_1$ and $^2A_1$ Terms in the CrO_4^{3-} Cluster for Different Combinations of Basis Sets Specified in the Text

	RCC + DK3		RCC + RCC		ECP + ECP	
	CASSCF	CASPT2	CASSCF	CASPT2	CASSCF	CASPT2
gas phase	−1461	−826	−1461	−826	−1415	−823
crystal	1112	1936	1346	2276	658	1184
Δ_{G-C}	2573	2762	2807	3102	2073	2007

by 0.18 Å, in order to match other interatomic distances revealed by EXAFS, the relaxation of neighboring CO_3^{2-} ions was supposed, the main feature being the rotation of Mn−O(1)−C planes by 20°.[42] The recent ligand-field (LF) simulations of optical transitions and EPR in $CaCO_3$:Mn^{2+} [43]

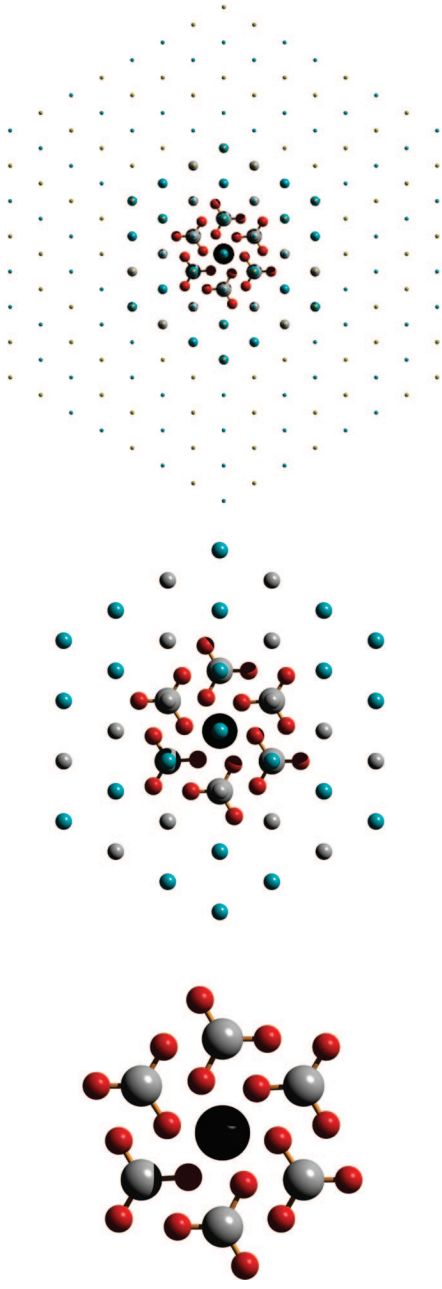

Figure 3. Schematic representation of the cluster $Mn(CO_3)_6^{10-}$ (bottom) embedded into two layers of CO_3^{2-} FAIMP (large balls) and two layers of Ca^{2+} AIMP (small balls) (middle) and eight layers of point charges (top). The view is along the 3-fold symmetry axis.

have further refined the geometry of six oxygens surrounding the manganese ions; however, the structural changes were found to be rather small. In the following, we adopted a simplified structural model for the manganese impurity, which only included the relaxation of the Mn−O bond by 0.18 Å, while all other nuclear coordinates were left unchanged.

We performed CASSCF/CASPT2 calculations of the $Mn(CO_3)_6^{10-}$ cluster (Figure 3, bottom) with Cowan−Griffin relativistic core model potentials with a [3s3p4d] contraction for Mn,[33] a [2s3p1d] contraction for carbon, and a [2s4p1d] contraction for oxygen. The embedding into the calcite lattice was simulated by two layers of FAIMPs (or atomic AIMPs for performance comparison with the AIMP method) on CO_3^{2-} ions and two layers of AIMPs on Ca^{2+} ions around the central cluster (Figure 3, middle) and seven layers of point charges replacing these two types of ions (Figure 3, top). For the CO_3 fragments, two different FAIMPs were constructed and optimized corresponding to two orientations of the carbonates in the calcite crystal. The five unpaired electrons on the Mn^{II} impurity make the $^6A_1$ ground state, relative to which the first 24 quartet LF excited states were calculated. For the LF states, a minimal active space was employed, consisting of five 3d orbitals of manganese and an additional five double-shell orbitals, that is, five electrons in 10 orbitals of active space. Dynamical correlation effects were computed at the CASPT2 stage by correlating all electrons (the core–electrons were represented by ECP). To reduce the computational effort for these calculations, the virtual space was reduced by 200 orbitals out of a total of 470 functions. Besides LF excitations, the lowest ligand-to-metal charge transfer (LMCT) state was evaluated as well with both atomic AIMPs and FAIMPs in the same environment and with an enlarged active space. The relatively large size of the ligands leads to a closely spaced manifold of molecular orbitals; therefore, in order to have converged CASSCF and CASPT2 calculations, it was necessary to use a rather extended active space of 35 electrons in 20 orbitals.

The results of the calculations are shown in in Table 2. The first column in the table shows the free ion Mn(II) parentage of the LF terms, which is meaningful given that the weak ligand-field scenario is realized in the complex $Mn(CO_3)_6^{10-}$.[43] The trigonal symmetry of the cluster and the environment require that the T terms split into nondegenerate A and double degenerate E representations of the trigonal symmetry group, which can be easily recognized in the results. Comparison with the assigned transitions of the optical absorption spectra for Mn^{2+} ions in shells[43] shows differences with the calculated values in Table 2 of several thousand wavenumbers. This is probably explained by the nonoptimized geometry of the impurity center and the poor

Table 2. Energies (cm^{-1}) of LF and LMCT Excited States of the $Mn(CO_3)_6^{10-}$ Cluster Calculated with AIMP and FAIMP Methods

			AIMP		FAIMP	
		O_h	CASSCF	CASPT2	CASSCF	CASPT2
ligand field	^6S	$^6A_1$	0	0	0	0
	^4G	$^4T_1$	25256	22740	25325	22788
			25428	22947	25577	23075
			25428	22951	25577	23068
		$^4T_2$	28619	26936	28606	26905
			28894	27300	28996	27414
			28896	27308	28996	27410
		^4E	30055	28818	30059	28800
			30056	28809	30059	28808
		$^4A_1$	30167	28871	30189	28896
	^4D	$^4T_2$	35502	32240	35546	32271
			35502	32248	35546	32267
			35634	32423	35723	32501
		^4E	37407	34260	37337	34190
			37407	34263	37337	34196
	^4P	$^4T_1$	38466	35373	38358	35239
			38731	35768	38754	35771
			38732	35761	38754	35718
	^4F	$^4T_1$	49819	45764	49846	45760
			49819	45766	49846	45759
			50067	46060	50139	46110
		$^4A_2$	50578	45857	50605	45926
		$^4T_2$	52655	49187	52602	49104
			52656	49179	52603	49112
			52814	49356	52810	49355
LMCT		^6A	56739	94942	56157	93673

treatment at the CASPT2 level, which we were enforced to adopt. Another source of errors is the insufficient basis set on the manganese ion which, in particular, leads to the overestimation of the excitation energies to states with different spin multiplicities.[44] However, this drawback is not expected to affect much the assessment of the FAIMP method for this system.

The comparison of the results obtained by FAIMP and AIMP methods shows differences which do not exceed 100 cm^{-1} for the calculated energies, which are much lower than the differences obtained for $YVO_4:Cr^{5+}$ in the previous section. This is due to the fact that the ligands in the present case are much larger and, therefore, screen efficiently the short-range potential of the fragments. This is not expected to be so in the case of LMCT excitations. Indeed, as the last line of Table 2 shows, the effect of FAIMP is much stronger, giving the difference with the AIMP method of about 600 cm^{-1} for the CASSCF and 1300 cm^{-1} for the CASPT2 calculation. This excitation corresponds to the transfer of one electron from a doubly occupied ligand orbital delocalized over two oxygens of the carbonate, one of them being the closest to the manganese ion (Figure 4a) and the other to the singly occupied 3d orbital of manganese (Figure 4b). As Figure 4a shows, there is a direct overlap of the ligand orbital with the nearest-neighbor CO_3 group from the first layer of the embedding, which makes its energy sensitive to the interaction with this group.

V. Conclusions

The fragment AIMP method is a useful generalization of the AIMP method. It permits a more accurate description of the

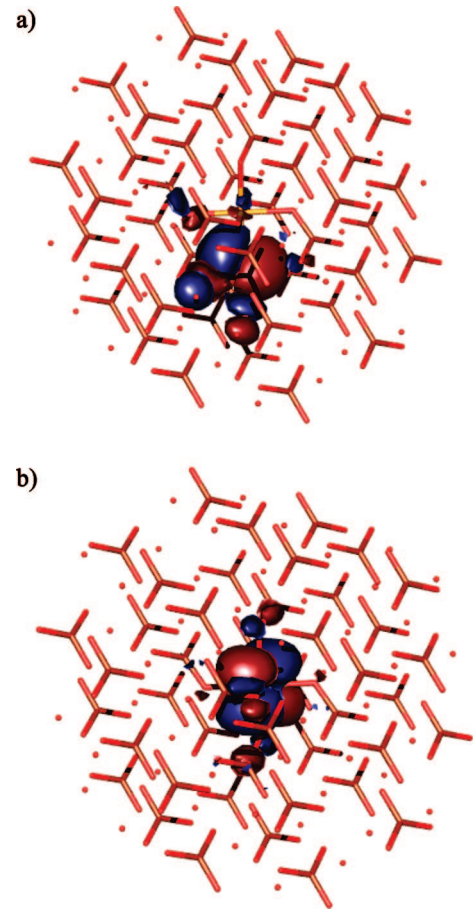

Figure 4. The ligand orbital (a) and the metal orbital (b) involved in the lowest LMCT of the $Mn(CO_3)_6^{10-}$ cluster.

(crystalline) environment of a molecular system without imposing limits on the frozen densities used to represent this environment. This opens the door for a more accurate treatment of the local states and the related spectroscopy in carbonates, sulfates and many natural minerals, molecular solids, and so forth. The method is also more flexible in its choice of basis sets for the fragments' atoms. These basis sets are also easier to construct. When used with single atom fragments, the method essentially reduces to the AIMP implementation. The main downside of this method is the fact that it is computationally more expensive, albeit only in the calculation of the one-electron integrals for the cluster. In subsequent calculations, FAIMP corrections are present in the one-electron matrices and do not increase the computational time in any way. The limiting step in the calculation of the FAIMP integrals is the contraction of the fragment density matrices with the two-electron interaction integrals. Test calculations for $YVO_4:Cr^{5+}$ and $CaCO_3:Mn^{2+}$ systems show that the corrections introduced by FAIMP treatment compared to the conventional AIMP method are important.

Consistent with the frozen environment approximation, nonlocal properties of perfect or imperfect crystals should not be the target of the FAIMP method as it is presented here. Furthermore, the extent or definition of the reference cluster should be consistent with the frozen environment approximation in the calculation of local properties. For dealing with more covalent hosts or very extended defects,

other alternative methods, which can be used along a building block route or as embedding methods, should be preferred.[25,45]

As already mentioned, the described implementation of the FAIMP method in the MOLCAS 7.0 package still lacks two essential features: (i) the AIMP representation of bielectronic and projection operators and (ii) the account of symmetry of the supermolecule (cluster + fragments). These are tasks for further development. Their accomplishment would greatly facilitate the use of the FAIMP method for embedded calculations, especially for the geometry optimization of impurity systems, which is done routinely for the AIMP method.

Acknowledgment. Financial support by the Flemish Science Foundation and the Flemish Government under the Concerted Action Scheme are gratefully acknowledged. B.S. thanks the MOLCAS group, while L.C. and M.H. would like to thank the Madrid group for hospitality during their visits.

References

(1) Sugano, S.; Shulman, R. G. *Phys. Rev.* **1963**, *130*, 517–530.

(2) Peeters, A.; Van Alsenoy, C.; Lenstra, A. T. H.; Geise, H. J. *Int. J. Quantum Chem.* **1993**, *46*, 73–80.

(3) Swerts, B.; Van Droogenbroeck, J.; Peeters, A.; Van Alsenoy, C. *J. Phys. Chem. A* **2002**, *106*, 4245–4250.

(4) Whitten, J. L. *Chem. Phys.* **1993**, *177*, 387–397.

(5) Barandiarán, Z.; Seijo, L. *J. Chem. Phys.* **1988**, *89*, 5739–5746.

(6) Seijo, L.; Barandiarán, Z. In *Computational Chemistry: Reviews of Current Trends*; Leszcynski, J., Ed.; World Scientific: Singapur, 1999; Vol. 4, pp 55–152.

(7) Maseras, F.; Morokuma, K. *J. Comput. Chem.* **1995**, *16*, 1170–1179.

(8) Huzinaga, S.; Cantu, A. A. *J. Chem. Phys.* **1971**, *55*, 5543–5549.

(9) Kleiner, M.; McWeeny, R. *Chem. Phys. Lett.* **1973**, *19*, 476–479.

(10) Katsuki, S. *J. Chem. Phys.* **1993**, *98*, 496–501.

(11) Mejias Romero, J. A.; Sanz, J. F. *J. Chem. Phys.* **1993**, *99*, 1255–1261.

(12) Ohta, K.; Yoshioka, Y.; Morokuma, K.; Kitaura, K. *Chem. Phys. Lett.* **1983**, *101*, 12–17.

(13) von Arnim, M.; Peyerimhoff, S. D. *Theor. Chim. Acta* **1993**, *87*, 41–57.

(14) von Arnim, M.; Peyerimhoff, S. D. *Chem. Phys. Lett.* **1993**, *210*, 488–494.

(15) Colle, R.; Salvetti, O. *Theor. Chim. Acta* **1991**, *80*, 63–70.

(16) Colle, R.; Curioni, A.; Salvetti, O. *Theor. Chim. Acta* **1993**, *86*, 451–465.

(17) Durand, Ph.; Malrieu, J. P. In *Advances in Chemical Physics: Ab Initio Methods in Quantum Chemistry*; Lawley, K. P., Ed.; Wiley: New York, 1987; vol. *LXVII*, part I, p 321.

(18) Poteau, R.; Ortega, I.; Alary, F.; Ramirez Solis, A.; Bartelat, J. C.; Daudey, J. P. *J. Phys. Chem. A* **2001**, *105*, 198–205.

(19) Carissan, Y.; Bessac, F.; Alary, F.; Heully, J. L.; Poteau, R. *Int. J. Quantum Chem.* **2006**, *106*, 727–733.

(20) Parr, R. G.; Elisson, F. O.; Lykos, P. G. *J. Chem. Phys.* **1956**, *24*, 1106.

(21) Note that, in general, the cluster basis set does not include basis functions of elements that belong to the environment. However, in some particular cases, the cluster basis set should be enlarged so as to include basis functions of next neighbours. This is only necessary in cases where geometry optimizations are done with respect to coordinates that confront cluster and environment components along bonding directions of the cluster (ref 6) or in cases where delocalized cluster states are calculated, such as impurity-trapped excitons.[22] None of these cases apply here.

(22) Ordejón, B.; Seijo, L.; Barandiaran, Z. *J. Chem. Phys.* **2007**, *126*, 194712.

(23) Pople, J.; Krishnan, R.; Schlegel, H. B.; Binkley, J. S. *Int. J. Quantum Chem.* **1979**, *S13*, 225.

(24) MOLCAS 7.0: Karlström, G.; Lindh, R.; Malmqvist, P.-A.; Roos, B. O.; Ryde, U.; Veryazov, V.; Widmark, P.-O.; Cossi, M.; Schimmelpfennig, B.; Neogrady, P.; Seijo, L. *Comput. Mat. Sci.* **2003**, *28*, 222–239.

(25) Whitten, J. L.; Yang, H. *Surf. Sci. Rep.* **1996**, *24*, 55.

(26) Baglio, J. A.; Gashurov, G. *Acta Crystallogr., Sect. B* **1968**, *24*, 292–293.

(27) (a) Banks, E.; Greenblatt, M.; Post, B. *Inorg. Chem.* **1970**, *9*, 2259–2264. (b) Albrecht, C.; Cohen, S.; Mayer, I.; Reinen, D. *J. Solid State Chem.* **1993**, *107*, 218–228.

(28) Greenblatt, M.; Pifer, J. H. *J. Solid State Chem.* **1979**, *29*, 1–7.

(29) Hazenkamp, M. F.; Stückl, A. C.; Cavalli, E.; Güdel, H. U. *Inorg. Chem.* **2000**, *39*, 251–254.

(30) Pascual, J. L.; Barandiarán, Z.; Seijo, L. *Int. J. Quantum Chem.* **2002**, *90*, 751–758.

(31) Evjen, H. M. *Phys. Rev.* **1932**, *39*, 675–687.

(32) Roos, B. O.; Lindh, R.; Malmqvist, P.-A.; Veryazov, V.; Widmark, P.-O. *J. Phys. Chem. A* **2004**, *108*, 2851–2858.

(33) Barandiarán, Z.; Seijo, L. *Can. J. Chem.* **1992**, *70*, 409–415.

(34) Petterson, L. G. M. Private communication.

(35) Tsuchiya, T.; Abe, M.; Nakajima, T.; Hirao, K. *J. Chem. Phys.* **2001**, *115*, 4463–4472.

(36) Barandiarán, Z.; Seijo, L.; Huzinaga, S. *J. Chem. Phys.* **1990**, *93*, 5843–5850.

(37) Seijo, L.; Barandiarán, Z.; Huzinaga, S. *J. Chem. Phys.* **1989**, *91*, 7011–7017.

(38) Roos, B. O.; Taylor, P. R.; Siegbahn, P. E. M. *Chem. Phys.* **1980**, *48*, 157–173.

(39) Andersson, K.; Mamlqvist, P.-A.; Roos, B. O.; Sadlej, A. J.; Wolinski, K. *J. Phys. Chem.* **1990**, *94*, 5483–5488.

(40) Andersson, K.; Mamlqvist, P.-A.; Roos, B. O. *J. Chem. Phys.* **1992**, *96*, 1218–1226.

(41) Marshall, S. A.; Serway, R. A. *Phys. Rev.* **1968**, *171*, 345–349.

(42) Cheng, L.; Sturchio, N. C.; Bedzyk, M. J. *Phys. Rev. B: Condens. Matter Mater. Phys.* **2001**, *63*, 144104.

(43) Cheng, L.; Xiao-Yu, K.; Xiao-Ming, T.; Xiong, Y. *J. Phys. Chem. A* **2007**, *111*, 2783–2789.

(44) Pierloot, K.; Vancoillie, S. *J. Chem. Phys.* **2006**, *125*, 124303.

(45) Seijo, L.; Barandiarán, Z. *J. Chem. Phys.* **2004**, *121*, 6698.

CT7003148